Comparative studies of hybrid functional materials based on different carbon structures decorated with nano-magnetite. Suitable application as platforms for enzyme-free electrochemical sensing of hydrogen peroxide

Lisandro Venosta [a], María V. Bracamonte [a]*, Marcela C. Rodríguez [b], Silvia E. Jacobo [c], Paula G. Bercoff[a]*

[a] Facultad de Matemática, Astronomía, Física y Computación (FaMAF). Universidad Nacional de Córdoba. IFEG, CONICET. Medina Allende s/n, Ciudad Universitaria, Córdoba, Argentina.

[b] Facultad de Ciencias Químicas, Universidad Nacional de Córdoba. INFIQC, CONICET. Haya de la Torre s/n, Ciudad Universitaria, Córdoba, Argentina.

[c] DiQuiMMAI, Facultad de Ingeniería, Universidad de Buenos Aires. INTECIN, CONICET. Av. Paseo Colón 850, Buenos Aires, Argentina

*vbracamonte@famaf.unc.edu.ar; bercoff@ famaf.unc.edu.ar

Abstract

A simple synthesis procedure was designed to obtain hybrid materials based on graphite structures and magnetite nanoparticles. These new structures were characterized using different techniques. The results show that the graphite structures were densely decorated by spherical Fe_3O_4 nanoparticles. The amount of immobilized magnetite was controlled by the number of defects present in the different pristine graphite materials.

The electro-catalytic behavior of modified glassy carbon electrodes, using magnetite-graphite hybrids exhibited an enhanced catalytic ability towards H_2O_2 reduction. The best response was obtained using graphites with smaller particle sizes (2 μm and 17 μm), modified with nano-magnetite. The performance of the electrode in terms of sensitivity for H_2O_2 amperometric detection was (1.1 ± 0.1) x 10^5 μA M^{-1} cm^{-2} mg^{-1} while the LOD was 0.50 nM at a working potential of -0.200 V. These values are comparable to those obtained using carbon nanotubes and metal or metal-oxide based sensors. The new proposed material appears as a very promising alternative for H_2O_2 non-enzymatic sensors mainly because its low cost and abundance. Also, the comparison between the different carbon substrates highlights the importance of the close contact between carbon and nano-magnetite, which enhances the catalytic behavior of the material.

Keywords: magnetite • graphite • hybrid material • hydrogen peroxide • sensor

1. Introduction

Recently, the need for new specific functions has contributed to the increase in the research and development of novel materials. In the last few decades, hybrid multifunctional materials have become a new type of multipurpose platforms with very important and promising applications in a wide spectrum of scientific and technological areas such as spintronics, energy production and storage, catalysts, and sensing or biosensing devices [1,2], among others. Some of the most successful hybrid materials belong to the group of composites, which are formed by the combination of a basic structural material, called the building blocks (filler) into a second substance, named the matrix (host) [3,4]. The research on hybrid multifunctional materials has become a central task, since it has been shown that the combination of host and filler originates novel fascinating functional materials with more complexity and superior properties compared to those of the pure counterparts [5]. Nowadays, the most studied hybrid materials result from the combination of nano-building blocks from inorganic nature and organic matrices, such as the case of metallic nanoparticles and polymers, biomolecules or even liquid media [6]. In addition, new hybrid

materials with tunable properties which respond to external stimuli mimicking the organisms functions are of particular interest in specific applications, such as biosensing strategies [7,8].

Nanomaterials in general exhibit conspicuous properties such as fast electron transfer kinetics, high surface-to-volume ratio, outstanding biocompatibility, chemical stability and easier routes for biomolecular coupling. Therefore, nanomaterials are excellent tools for improving a number of applications like solar cells [9], magnetic resonance imaging [10], and biorecognition and transduction steps in sensing strategies [7]. Likewise, nanomaterials of distinctive nature display highly efficient enzyme-like activity in a wide range of non-physiological conditions, such as extreme pH values, high temperature or in the presence of inhibitors. Among the most used nanosized materials, iron oxide has been mostly studied because it is environmentally safe, non-toxic, heat and corrosion-resistant and a cost-effective material [11]. In particular, magnetite (Fe_3O_4) and maghemite (γ-Fe_2O_3) nanoparticles have attracted much interest due to their magnetic properties [12,13] in the field of sensing materials [14,15]. Additionally, magnetite nanoparticles have demonstrated intrinsic peroxidase-like activity and have been applied as peroxidase nanomimetics to detect a wide range of biomolecules. Nanosized particles of numerous magnetic materials have been incorporated into extended matrix materials (i.e., organic or inorganic polymers) to create hybrid functional systems with magnetic properties. In this sense, several studies related to immobilization of magnetite onto different substrates have been carried out; in particular combining magnetite nanoparticles with carbon materials such as nanotubes [16], carbon fibers [17], fullerenes [18] and grapheme [19]. However, to the best of our knowledge, there are not systematic studies about the use of bulk graphite as support for nano-magnetite.

Bulk graphite is a well-known material, with thermal and electric conductivities that depend on the relative direction of the stacking layers of graphene. Graphite materials are widely used in electroanalysis since they have a broad potential window, low baseline current, high density of surface functional groups and low cost. Additionally, they are chemically inert and can be used for the construction of diverse sensors and detectors [20].

Hydrogen peroxide (H_2O_2) is a strong oxidizing agent and its applications are widely extended in chemical, textile, pharmaceutical and alimentary industries [21-23]. In addition, H_2O_2 is a unique marker for a number of biological and environmental processes [24,21]. H_2O_2 has become a significant cytotoxic chemical related to the severe damage of human health. Under the influence of environmental stress factors and/or genetic mutations, the mitochondria trigger disproportionate H_2O_2 production. The long-term exposure to H_2O_2 has been connected to serious diseases such as ageing cells, cancer and neurodegenerative processes like Alzheimer, Parkinson and Huntington [25,26]. Therefore, the requirements for the monitoring of very low levels of H_2O_2 may be achieved by the implementation of highly sensitive sensing systems. Several methods for H_2O_2 detection have been lately employed including titrimetry, spectrophotometry, chromatography, chemiluminescense and electrochemical techniques [27]. Among these methods, electrochemistry offers the lowest cost/benefits ratio since it requires small and low-cost instrumentation with operational simplicity displaying high sensitivity, fast and accurate detection. For this purpose, a number of enzyme-based electrochemical sensors have been proposed [28]. However, enzymatic sensors imply higher costs of fabrication, shorter shelf-life due to enzyme lack of long-term stability in media reaction and poor reproducibility, requiring extra operational precautions. In this sense, the detection of H_2O_2 is an extremely important challenge for speeding-up the design of new electrochemical sensing platforms with intrinsic peroxidase-like activity.

In this work we report a systematic study of several graphitic materials, with different particle sizes, used as support for magnetite nanoparticles to obtain magnetite∩graphite hybrids. The obtained hybrids are characterized and evaluated electrochemically taking advantage of the peroxidase-like catalytic activity of magnetite, as a function of the carbon substrate. Also, the catalytic performance of the nano-magnetite∩graphite hybrids was compared to nano-magnetite∩carbon-nanotubes hybrids, showing a comparable behavior. This result may open the window to the use of powder graphite as a promising alternative of scalable and low-cost substrates for magnetite nanoparticles in the design of sensing and biosensing electrochemical platforms with peroxidase nanomimetic catalytic activity.

2. Materials and Methods

2.1 Materials

Graphites of varied characteristics were purchased from different providers. Graphite powder (> 20 μm) and graphite flakes (> 300 mesh) were purchased from Sigma. Graphite Micrograf was from Nacional de Grafito (99503UJ > 2.74 μm). Expandable graphite was obtained from Sigma Aldrich (+ 50 mesh). To have a smaller particle size, the expandable graphite was manually milled for 3 h using an agate mortar, obtaining a mean particle size of 120 μm. Multi wall carbon nanotubes (9.5 nm diameter and 1.5 μm length, <95 % purity) were purchased from Nanocyl (www.nanocyl.com). Iron (II) sulphate heptahydrated was from Sigma and Iron (III) chloride hexahydrated was from Anedra. Hydrogen peroxide (30 % V/V aqueous solution), Na_2HPO_4 and NaH_2PO_4 were provided by Baker. Ammonia chloride and hydrochloric acid were from Cicarelli. Other chemicals were reagent grade and used without further purification. All solutions were prepared with ultra-pure water (18 MOhm cm) from a Millipore MilliQ system. Stock solutions of 0.2 M Fe^{2+} and 0.1 M Fe^{3+} were prepared by dissolving $FeSO_4 \cdot 7H_2O$ and $FeCl_3 \cdot 6H_2O$ into 2 M HCl aqueous solutions, respectively.

2.2 Characterization methods

X-ray diffraction (XRD) patterns were obtained in a Philips PW1800/10 diffractometer operated at 40 kV and 30 mA with a Cu-Kα radiation source. Scanning electron microscopy (SEM) images were obtained with a field emission scanning electron microscope FE-SEM, Sigma Zeiss (LAMARX facilities) working at 5 kV. Transmission electron microscopy (TEM) images were obtained using a Hitachi HT7700 high resolution TEM, with 100 keV. Energy dispersive X-ray spectroscopy was performed using an Oxford detector attached to the microscope. The mean particle size of each sample was statistically determined by measuring distances on several SEM images corresponding to the carbon without magnetite. The results were used to generate the samples nomenclature, as shown in **Table 1**, being the number of each label the mean particle size, in microns.

Raman spectra were measured with a laser Raman spectrophotometer (Confocal Horiba Jobin-Yvon LabRam HR) with an excitation wavelength of 633 nm.

Electrochemical measurements were performed with a TEQ 04 potentiostat and Autolab 302N (Autolab, Methrom). The electrodes were inserted into the cell (BAS, Model MF-1084) through holes in its Teflon cover. A platinum wire and Ag/AgCl, 1 M KCl (CHI, Model 111) were used as counter and reference electrodes, respectively.

A vibrating-sample magnetometer (VSM, *Lake Shore 7300*) was used to study the magnetic properties of the samples. The magnetization hysteresis loops were measured in fields between ±0.9 T, at room temperature.

2.3 Electrochemical measurements

A glassy carbon electrode (GC electrode, Model 104, CH Instruments, 3 mm) was used as working electrode. GC electrode was cleaned by polishing (prior to surface modification) with 1.0 and 0.3 mm alumina slurries (micropolish Buehler) for 2 min and then washed with Milli-Q water.

Hybrid inks containing Fe_3O_4∩graphite or CNTs were prepared by dispersing 1.0 mg of the different hybrid powders in 1.0 mL of 0.1 % Nafion® in 50/50 ethanol/water solution. In each case the mix was sonicated for 30 min until a homogeneous dispersion was obtained. Finally, 10.0 μL of prepared ink was placed on the GC electrode surface and allowed to dry. Catalytic electrodes obtained from diverse deposition batches and screened under identical conditions were found to display a performance variability of < 10 % in terms of current density.

3. Results and Discussion

3.1 Synthesis of magnetite and magnetite∩carbon hybrid materials

Magnetite (Fe_3O_4) nanoparticles (NPs) were synthesized by an ultrasonic-assisted co-precipitation method [29]. In a typical procedure, 1.0 mL of 0.20 M $FeSO_4$ solution and 4.0 mL of 0.10 M $FeCl_3$ solution were mixed. The mixed Fe^{2+}/Fe^{3+} solution was sonicated for 30 min in an ultrasonic cleaning bath (sonic bath Testlab, TB02, 40 kHz with a power of 80 W). Afterwards, 18.0 mL of 0.70 M ammonia were added drop-wise to the mixture and sonicated for another 30 min. The generated black Fe_3O_4 NPs were collected by magnetic separation and washed first with water until reaching neutral pH and then with acetone. Afterward, the NPs were filtered and dried at 80 °C in vacuum for 18 h. When the carbon material is used as support for the magnetite NPs, it is included during the first step of the synthesis, mixing 0.30 g of the graphite with the Fe^{2+}/Fe^{3+} solution. The following procedure of the synthesis is the same as described above. The obtained samples of hybrid materials were labeled Fe_3O_4∩G*xyz*, being *xyz* the number corresponding to the graphite particle size, in micrometers (see **Table 1** below).

3.2 Physicochemical characterization of the hybrids

SEM/EDX analyses were performed in order to investigate the overall morphology and elemental composition of the hybrid materials. **Figure 1** displays the SEM images obtained for the samples of magnetite NPs decorating the different graphites.

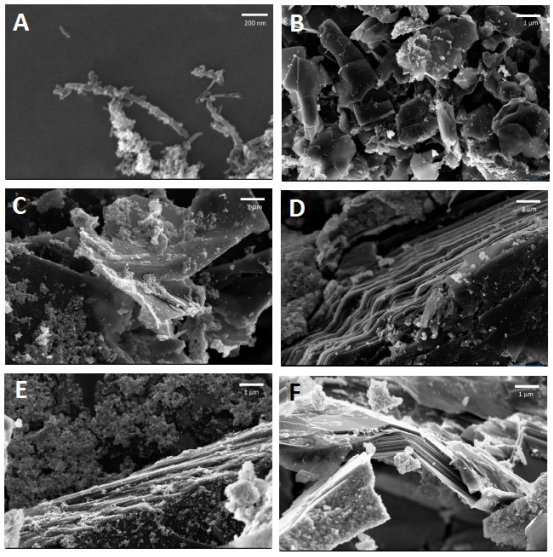

Figure. 1. SEM images of Fe_3O_4∩CNTs (**A**), Fe_3O_4∩G002 (**B**), Fe_3O_4∩G017 (**C**), Fe_3O_4∩G120 (**D**), Fe_3O_4∩G390 (**E**) and Fe_3O_4∩G410 (**F**). The bar corresponds to 200 nm in (A) and to 1μm in the other images.

The mean particle size of all graphites was determined from several images of each sample, using the Gwyddion software, and is given in **Table 1**. Figure S1 in Supplementary Information displays the corresponding histograms.

In **Figure 1**, Fe_3O_4 NPs are seen as bright spots. Even when the NPs appear to be homogeneously distributed on the carbon surface, several EDX-maps (Figure S2 shows a representative one) allowed us to determine that the magnetite NPs are mainly immobilized on the edges of the structures. This result is in good agreement with the major reactivity reported at the edges of carbon-based materials [30]. TEM images of loose Fe_3O_4 nanoparticles were used to determine an average size of (14 ± 2) nm for the magentite. Figure S3 in Supplementary Information displays the corresponding image and histogram.

Table 1. Particle size and nomenclature of the different used

Carbon material	Sample	Particle size
Expandable graphite	G410	410
Graphite	G390	390
Expandable graphite (milled)	G120	120
Graphite powder	G017	17
Graphite Micrograph	G002	2
Multi-wall carbon nanotubes	CNTs	-

3.3 XRD characterization

In order to confirm that the iron oxide on the carbon structures is magnetite, X-ray diffractograms of the resulting hybrid materials were performed, and the obtained results are shown in **Figure 2**. The diffractogram of the obtained magnetite NPs is included for comparison.

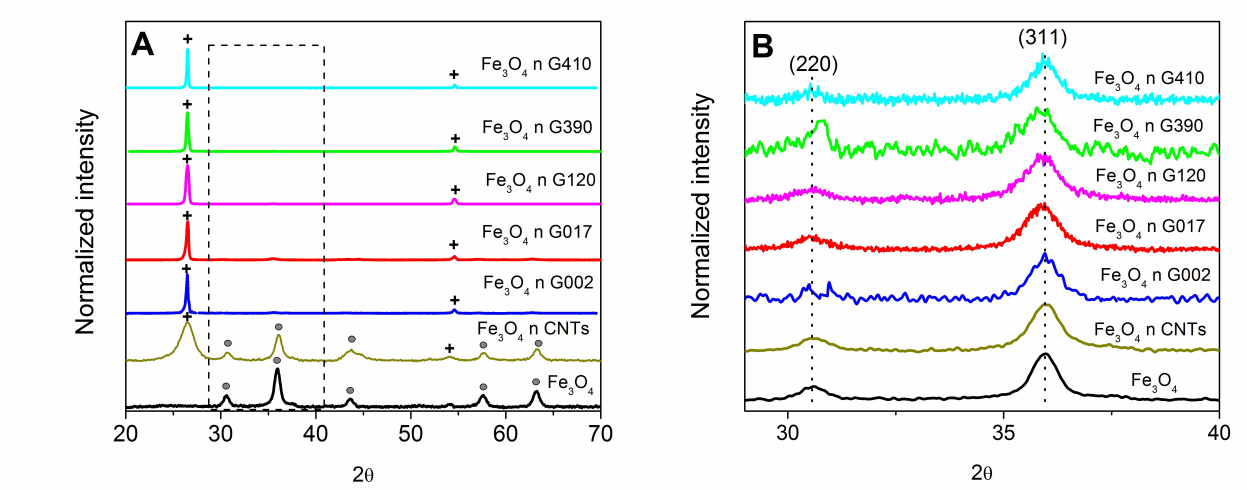

Figure 2. A) XRD patterns of pure Fe_3O_4 NPs and all the hybrids. Reflections (200) and (100) of graphite are indexed with (+) and the peaks corresponding to the spinel phase of magnetite are indexed with (●).**B)** Zoom of figure A showing the characteristic peaks corresponding to reflections (220) and (311) of magnetite.

The diffractogram of magnetite exhibits peaks at 2θ = 30.6º, 35.9º, 43.4º, 57.4º and 63.0º, corresponding to the crystal planes (220), (311), (400), (511) and (440) of the spinel structure (marked with solid circles in the diffractogram of **Figure 2 A**). All the samples containing graphite show a peak around 2θ = 27º which is associated to the graphite (200) diffraction line. In the case of Fe_3O_4∩CNTs, two peaks are observed at 2θ = 26.3° and 43.5°, which are related to reflections of (200) and (100) crystallographic planes of CNTs, respectively. The diffraction lines typical of the cubic crystal structure of magnetite are also present in the hybrids, confirming magnetite immobilization on every carbon substrate. The crystal size of magnetite was estimated using the Scherrer formula giving a value of ~10 nm, in good agreement with TEM results.

3.4 Magnetic measurements

Once the immobilization and the nature of the iron oxide present in the hybrid materials were confirmed, the quantification of magnetite in each sample was determined by measuring the specific magnetization (*M*) as a function of the applied magnetic field (*H*) (**Figure 3**). In every case, a typical superparamagnetic behavior ─marked by a slow approach to saturation and the absence of coercivity and remanence─ is observed. The highest specific magnetization was measured for magnetite NPs (69.2 emu g^{-1}) and is in good agreement with previous reports for this phase [31,32].

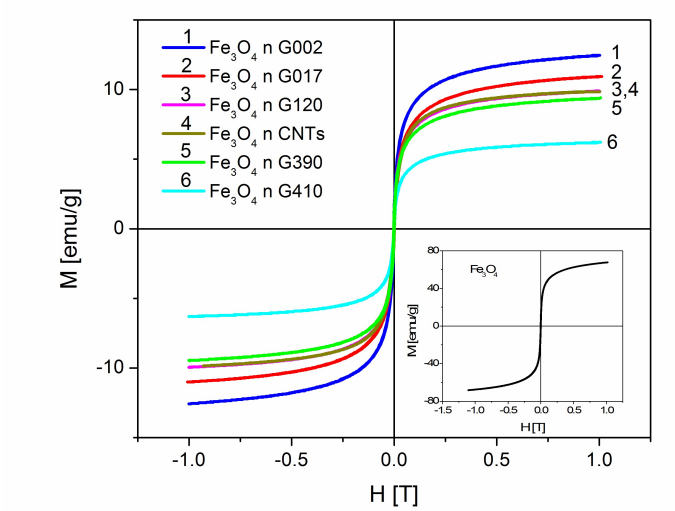

Figure 3. Hysteresis loops of all the studied hybrids. *Inset*: hysteresis loop of Fe_3O_4 NPs

Based on the above mentioned results ─which evidence no differences in the Fe_3O_4 crystal structure─ we calculated the amount of magnetite present in each hybrid by considering the maximum magnetization of pure Fe_3O_4 as corresponding to 100 percent magnetite content. The assessed values for each sample are listed in **Table 2**. Pure graphite samples exhibited a negligible diamagnetic behavior in every case.

Table 2. Magnetite content in each sample

Sample	Magnetite content [wt%]
Fe_3O_4∩G410	9
Fe_3O_4∩G390	14
Fe_3O_4∩G120	15
Fe_3O_4∩G017	16
Fe_3O_4∩G002	18
Fe_3O_4∩CNTs	14

3.4 Raman spectroscopy

Magnetite NPs and the hybrid materials synthesized by the ultrasonic-assisted co-precipitation method were also characterized by Raman spectroscopy. **Figure 4 A** shows the Raman spectra of the different materials. The spectrum of Fe_3O_4 NPs, at the bottom of **Figure 4 A**, shows the first-order characteristic major bands of magnetite at 350 cm^{-1} (E_g), 500 cm^{-1} ($T_{2g}(2)$) and 700 cm^{-1} (A_{1g}) [33,34]. The modes above

600 cm^{-1} represent vibrations in the tetrahedral sites of the spinel structure while the other low-frequency modes correspond to the octahedral sublattice. The hybrids present not only the characteristic D and G peaks of a graphitic material around 1550 cm^{-1} and 1350 cm^{-1}, respectively, but also the characteristic peaks of magnetite, marked with (*) in **Figure 4 B**. The appearance of the bands corresponding to both the substrate (C sp^2) and the magnetite, further support that the hybrids have been successfully formed.
The large line widths (~50-100 cm^{-1}) of the observed Raman bands of magnetite are related to a strong electron-phonon coupling [33] and small particles sizes [35]. A shoulder-like feature is noticed in the A_{1g} band around 700 cm^{-1}, indicating lattice defects, or loss of symmetry at tetrahedral sites [36]. Remarkably, the intensity of this peak is strongly dependent on the substrate of the hybrid. Trying to understand this effect, the relative intensity of the A_{1g} peak, normalized by the magnetite amount, was analyzed for each sample. The results, presented in **Figure 4 C**, show a decrease of the peak intensity for substrates with smaller particle sizes, independently of the amount of magnetite. We relate this decrease in the A_{1g} band intensity to a stiffening of the lattice in tetrahedral Fe-O bonds. This effect is possibly originated by a stronger interaction of the Fe atoms with the C atoms of the substrate [37], which might indicate a closer contact between the phases. According to this hypothesis, the most effective substrates for magnetite NPs' immobilization are G002 and G017. Carbon nanotubes are not included in this discussion because in this kind of nano-structure the curvature plays a special role in their reactivity, making the Raman interpretation a non-trivial problem.

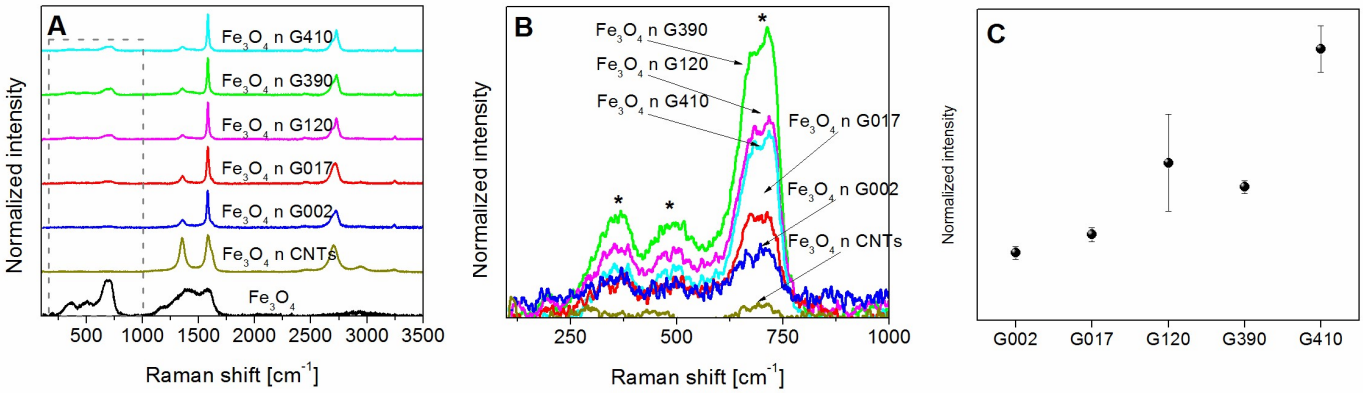

Figure 4. A) Raman spectra of the magnetite∩graphite hybrids using different carbon substrates: Fe_3O_4∩CNTs, Fe_3O_4∩G002, Fe_3O_4∩G017, Fe_3O_4∩G120, Fe_3O_4∩G390 and Fe_3O_4∩G410. The spectrum of pure magnetite NPs is also shown as a reference, at the bottom. The dashed rectangle indicates the region shown in B. **B)** Characteristic bands of magnetite, present in the spectra of all the hybrids. **C)** Relative intensity of magnetite A_{1g} mode in each sample.

A further assessment of the data was performed by analyzing the amount of magnetite immobilized on the carbon substrates as a function of the number of intrinsic defects present in the original pristine material. The number of defects was inferred from the intensity ratio between the D and G bands (I(D)/I(G)) of the carbon material prior to its modification with magnetite.[34] As shown in **Figure 5 A,** the amount of deposited Fe_3O_4 increases with the density of defects. Further analyses were performed studying the effect of the distance between defects (L_D) ─estimated using the Tunistra Koenig equation [38] ─ on the amount of immobilized magnetite. **Figure 5 B** shows that the smallest the distance L_D, the largest the percentage of Fe_3O_4, indicating that the defects are the main spot for the interaction between magnetite and the carbon substrate. The possible defects include edges, topological defects, vacancies, substitutional impurities and sp^3-like defects [39], which can be identified from the ratio between the D and D' bands [40]. In our case, the typical I(D)/I(D') value for every carbon substrate was around 2.5, indicating edges and/or topological-type defects in every sample.

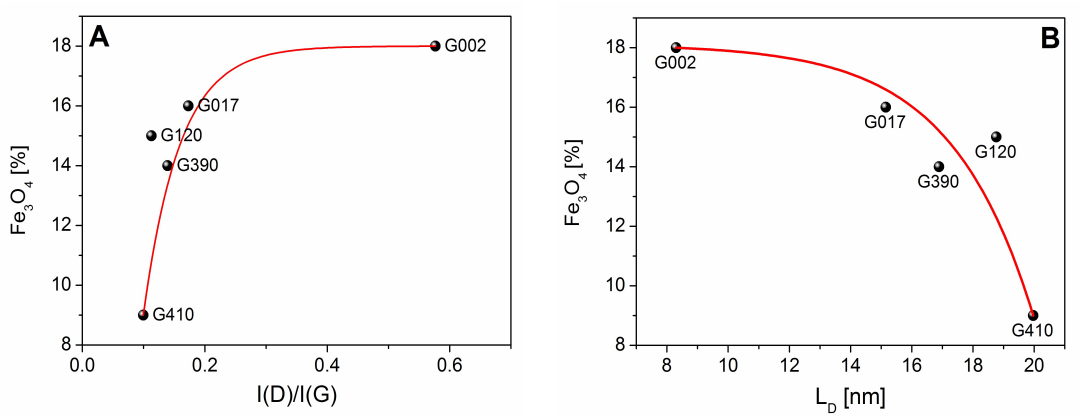

Figure 5. A) Amount (wt%) of magnetite immobilized onto different carbon substrates as a function of the I(D)/I(G) ratios. **B)** Distance between defects (L_D) of the carbon material prior to its modification with magnetite. The line is drawn as a guide to the eyes.

In conclusion, the detailed Raman analysis allowed us to confirm that the amount of magnetite deposited on each substrate depends on the defects density, being the carbon substrates with smaller particle sizes the more effective for Fe_3O_4 NPs immobilization. On the other hand, a stiffening of Fe-O tetrahedral bonds can be inferred from the intensity of the A_{1g} band, which may hint a closer contact between magnetite NPs and graphite in the hybrids with smaller particle size.

3.5 Characterization of the electrochemical response

Having noticed that the amount of magnetite deposited on the carbon substrates was different, we explored the electrochemical response of the hybrids, taking advantage of the peroxidase-like catalytic activity of magnetite. Cyclic voltammograms (CVs) experiments were carried out at 0.10 V s^{-1} in 0.10 M phosphate buffer solution pH 7.40, cycling the potential between -0.40 and 0.90 V in absence and presence of H_2O_2 (**Figure 6**).

From the curves measured without H_2O_2 (blank experiments, dashed lines) it is possible to infer that non-faradic currents are observed in the studied window potential, indicating the absence of electron transfer processes. In contrast, when the CVs are recorded in presence of H_2O_2 (red solid line), a marked cathodic response starts at potentials higher than -0.050 V. The currents recorded in this potential range are related to the H_2O_2 reduction to water. The dependence of the profile of H_2O_2 reduction on the nature of the hybrid material is remarkable. The determined onset potentials are listed in **Table 3**.

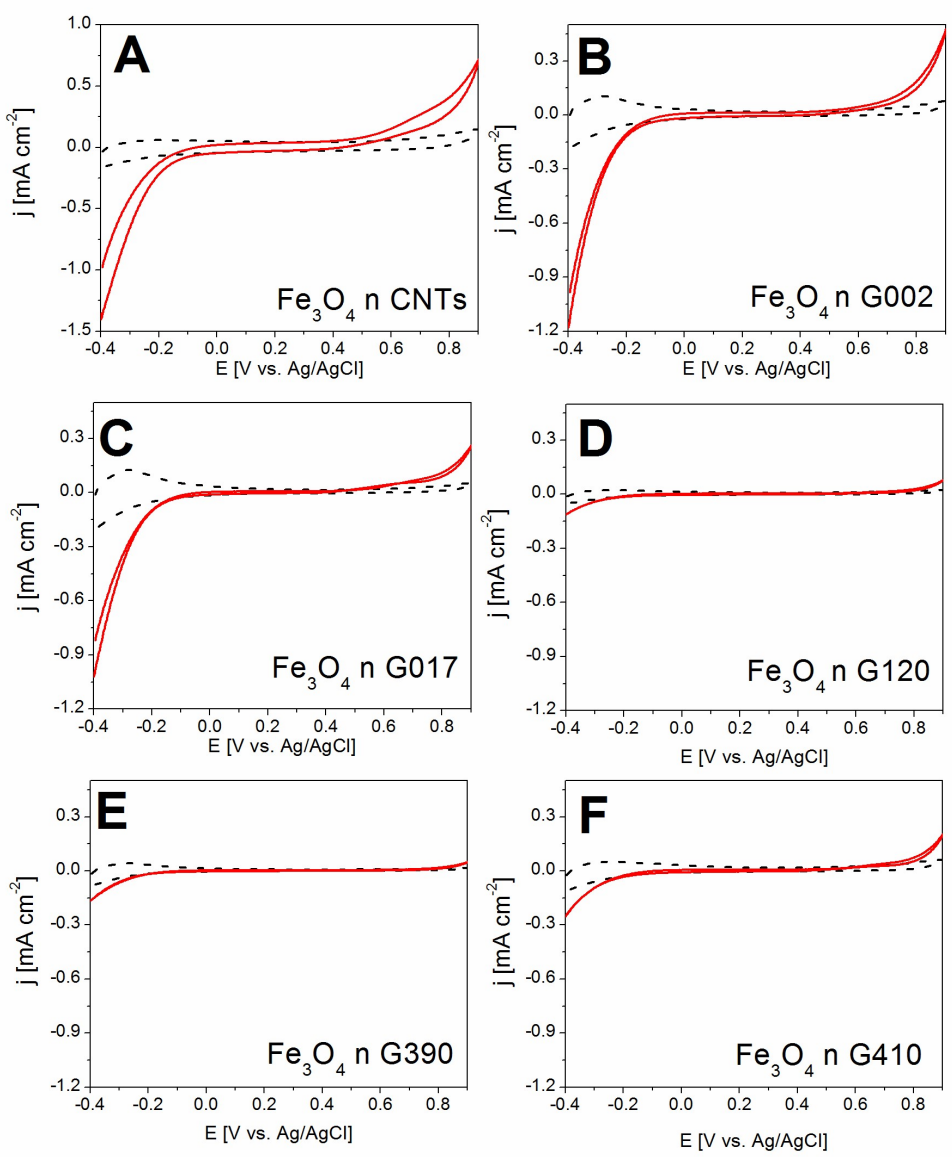

Figure 6. Cyclic voltammograms of Fe_3O_4∩CNTs (A), Fe_3O_4∩G002 (B), Fe_3O_4∩G017 (C), Fe_3O_4∩G120 (D), Fe_3O_4∩G390 (E) and Fe_3O_4∩G410 (F) in 0.10 M phosphate buffer solution without (black dashed line) and with (red solid line) 0.01 M H_2O_2. Scan rate: 0.10 V s^{-1}.

Table 3. Onset potentials and charge transfer resistance of the different hybrid materials.

	Hybrid material	Onset potential [V]	Rct [kΩ]
A	Fe_3O_4∩CNTs	-0.05	0.60 ± 0.07
B	Fe_3O_4G002	-0.06	0.57 ± 0.06
C	Fe_3O_4∩G017	-0.06	0.73 ± 0.04
D	Fe_3O_4∩G120	-0.25	19 ± 3
E	Fe_3O_4∩G390	-0.18	2.6 ± 0.4
F	Fe_3O_4∩G410	-0.18	4.7 ± 0.3

A significant decrease in the onset potential and an increase in the associated currents are observed when CNTs, G002 and G017 are used as substrates, highlighting the higher electro-catalytic ability of these hybrids upon the others. This effect is probably due to both, the remarkable high surface-to-volume ratio of the resultant composite and the improved conductivity of the carbon substrates. Studies using only the carbon supports in equivalent conditions were performed and the obtained reduction signals were much lower than in the presence of nano-magnetite (see **Figure S4** in Supplementary Information). Therefore, Fe_3O_4 with oxidation states of Fe (II) and Fe (III) was identified as the electro-catalyst responsible for H_2O_2 reduction. The proposed mechanism includes two-electron and two-proton assisted reductions with generation of H_2O as product. This process occurs in presence of H_2O_2 which is reduced when the oxidation of Fe (II) to Fe (III) takes place on Fe_3O_4, followed by the electrochemical regeneration of Fe (II) species at the electrode surface [41].

In order to have a deeper understanding of the hybrid materials electro-catalytic behavior, we studied their electrochemical impedance response in H_2O_2 solution. **Figure 7** shows the Nyquist plots obtained in 1.0 x 10^{-2} M H_2O_2 at -0.20 V for Fe_3O_4∩G002, Fe_3O_4∩G017, Fe_3O_4∩G120, Fe_3O_4∩G390, Fe_3O_4∩G410 and Fe_3O_4∩CNTs modified glassy carbon electrodes (GC electrodes). The equivalent circuit used to fit the impedimetric response is ($R_s(R_{ct}C_{dl})$) where the solution resistance (R_s) is in series with the charge transfer resistance (R_{ct}), which is in parallel with the constant phase element that represents the double layer capacitance (C_{dl}). R_s was constant with values of (11 ± 3) Ω while R_{ct} changed, depending on the material. The obtained results are presented in **Table 3** and reveal a significant lower charge-transfer resistance when CNTs, G002 and G017 are used as substrates, in good agreement with the voltammetric results. The lessening on both, the onset potential and the charge transfer resistance, can be attributed to a better electrical connection between the magnetite and the carbon substrate as the graphite size decreases. This observation is in good agreement with Raman results, which show a decrease in the intensity of the A_{1g} mode of magnetite, related to a stiffening of the lattice in tetrahedral sites because of interaction with the graphitic substrate.

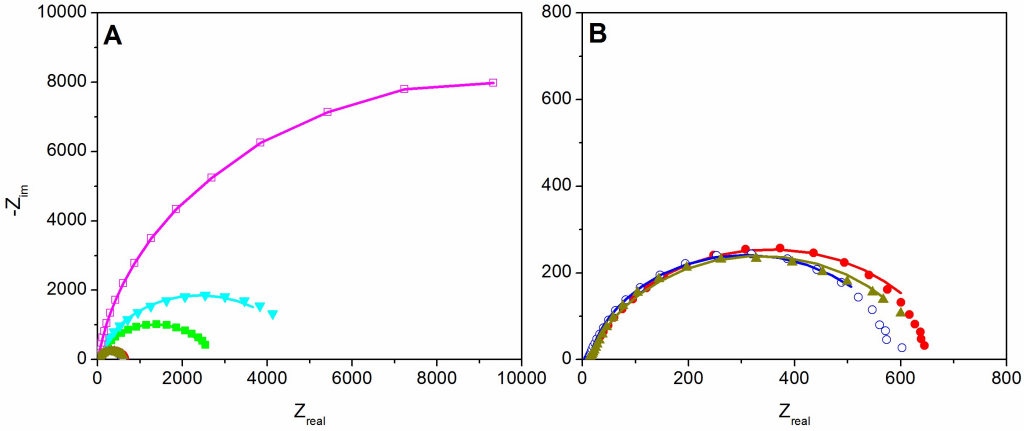

Figure 7. A) Nyquist plots obtained for Fe_3O_4∩CNTs (▲), Fe_3O_4∩G002 (○), Fe_3O_4∩G017 (●), Fe_3O_4∩G120 (□), Fe_3O_4∩G390 (■) and Fe_3O_4∩G410 (▼) modified GC electrodes. **B)** Zoom of the lower resistance responses presented in A. Points indicate the experimental data and lines the corresponding fit with the R(RC) circuit.

In order to evaluate the efficiency of the hybrid materials as possible catalytic agents in the development of non-enzymatic sensors, amperometric experiments were carried out at -0.200 V with the successive addition of H_2O_2 aliquots, in an electrochemical cell containing phosphate buffer solution pH 7.40. The optimum working potential for further experiments was selected from the hydrodynamic voltammograms obtained for 50.0 x 10^{-6} M hydrogen peroxide (**Figure S5** in Supplementary Information). For each material the reduction starts at −0.050 V and has an appreciable response at -0.200 V. **Figure S6** shows the calibration plots obtained from the amperometric recordings. The sensitivities of the different hybrids were calculated from the slopes of the calibration plots, and the results are presented in **Table 4**. Note that the sensitivity values are normalized by the magnetite content; other analytical parameters were included for a better comparison. Although Fe_3O_4∩CNTs has the highest sensitivity towards hydrogen

peroxide reduction (in agreement with the increase in the current density response observed in the voltammetric experiments, Figure 6) the sensing characteristics of Fe_3O_4∩G002 and Fe_3O_4∩G017 are of the same order than those obtained using carbon nanotubes as electrodic substrate, and even better than other systems previously reported [17,19b,41-45] (**Table S1** in Supplementary Information). Among the main advantages of these systems using graphite as electrodic substrates, it is possible to mention a very good analytical performance, lower cost and easier handling compared to the CNTs.

Table 4. Onset potentials and comparison of the analytical performance of the different H_2O_2 sensors.

Hybrid material	Sensitivity [x 10^5 µA M^{-1} cm^{-2} mg^{-1}][a]	LOD [nM][b]	Linear range [µM]
Fe_3O_4∩CNTs	(2.4 ± 0.5)	0.4	0.001 – 0.015
Fe_3O_4∩G002	(1.1 ± 0.1)	0.5	0.002 – 0.050
Fe_3O_4∩G017	(1.00 ± 0.06)	0.1	0.0003-0.025

[a] Normalized by the Fe_3O_4 content. [b] Calculated considering LOD=3.3 (σ/S) being σ the standard deviation of the blank and S the sensitivity.

The possible interference effects the most common easily oxidizable compounds usually present in biological fluids samples [46], such as ascorbic acid (AA), uric acid (UA) and acetaminophen (AP) were also evaluated. The amperometric experiments were carried out in 0.10 M phosphate buffer solution pH 7.40 by adding 0.025 mM H_2O_2, followed by three successive additions of 0.020 mM AA, 0.020 mM UA and 0.020 mM AP. **Figure 8** shows the amperometric response of potential interfering substances at the Fe_3O_4∩G017/GC electrode. As it was expected, the current responses of easily oxidable compounds are negligible; while a well-defined H_2O_2 response is obtained, indicating that the resulting amperometric sensor is highly selective for the detection of H_2O_2 in biological samples under physiological conditions. Analogous results were obtained using Fe_3O_4∩G002 and Fe_3O_4∩CNTs on GC electrodes (data not shown).

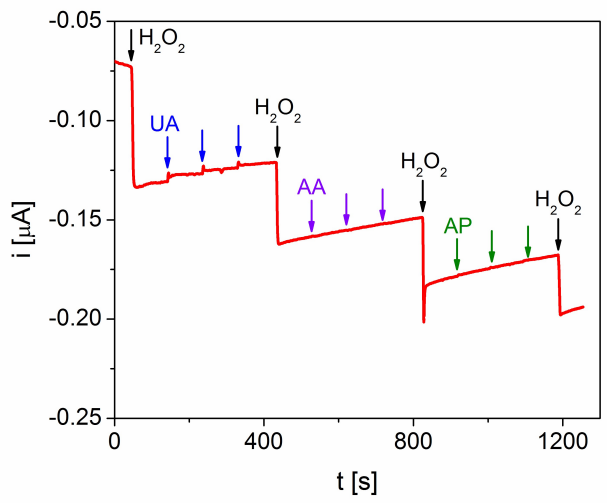

Figure 8. Amperometric responses of Fe_3O_4∩G017/GC electrode upon subsequent additions of 0.025 mM H_2O_2, 0.020 mM AA, 0.020 mM UA and 0.020 mM AP at -0.200 V vs. Ag/AgCl.

With the purpose of testing the possible matrix effects and interference in real samples, we studied the response of the magnetite∩graphite hybrids detecting H_2O_2 in a commercial UHT milk sample. The tested hybrids were: Fe_3O_4∩CNTs, Fe_3O_4∩G002 and Fe_3O_4∩G017. In the experimental setup, 4µL of milk were diluted in 10 mL of 0.10 M phosphate buffer solution (pH 7.40). Subsequently, a known amount of H_2O_2 was added, and its recovery was determined using amperometric measurements. The analyses indicate

recovery percentages of (105 ± 12) %, (99 ± 5) % and (108 % ± 9) for Fe_3O_4∩G002, Fe_3O_4∩G017 and Fe_3O_4∩CNTs, respectively. The presented data are calculated from 3 separate experiments. The obtained results indicate that the proposed electrodes are promising candidates for practical application in the determination of small amounts of H_2O_2.

We also investigated the reproducibility and stability of the electrodes modified with Fe_3O_4∩G017. For reproducibility studies, the amperometric response of five same short Fe_3O_4∩G017-modified GC electrodes were analyzed, yielding a relative standard deviation less than 10%. Next, three independent Fe_3O_4∩G017-modified GC electrodes were made to ascertain any batch-to-batch variability, and a relative standard deviation within 10% was also obtained. The stability was analyzed by measuring the sensitivity of calibration plots obtained from amperometric experiments at -0.200 V in the course of 14 days. The response of the sensor remained in 100% (SD ≤ 5%) after 9 days of consecutive assays from the date of preparation and first test. After two weeks of continuous use the response decays up to 80 % of the initial sensitivity (**Figure S7** in Supplementary Information). Considering these results, we can ascertain that the sensor exhibits a very good stability and preserves the catalytic activity towards H_2O_2 for repetitive experiments in a time span of over one week.

4. Conclusions

Fe_3O_4∩graphite hybrid materials were synthesized by co-precipitation, producing Fe_3O_4 nanoparticles of around 14 nm, dispersed on different graphite substrates and nanotubes surfaces. The amount of immobilized magnetite is associated to the number and kind of defects present in the pristine graphite materials. Raman analysis allows inferring that the more defects present in the sample, the higher the amount of immobilized magnetite. According to our interpretation of Raman spectra, a decrease in the intensity of the A_{1g} mode of magnetite is related to a stiffening of the lattice in tetrahedral sites because of interaction with the graphitic substrate. It is also observed that the more defects present in the sample, the higher the amount of immobilized magnetite.

The hybrid materials show a good catalytic response for H_2O_2 reduction evidencing a synergistic effect between the metal oxide and the graphite phases. The best catalytic behaviors using the graphites with smaller particle sizes as substrates are comparable to that of the CNTs. We propose that this enhancement ─ in contrast with carbon substrates of larger particles sizes ─ is related to the closer contact between magnetite NPs and graphite, concluded from Raman results. We proposed the design of a new enzyme-free sensing platform based on hybrid materials produced by combination of small particle size graphite and nano-magnetite as an alternative sensing strategy with lower cost, better handling, outstanding analytical performance and higher availability, comparable or even better than CNTs.

To the best of our knowledge this is the first example of a successful enzyme-free electrochemical sensor based on graphite decorated with magnetite NPs for H_2O_2 detection. The simplicity of preparation, the high sensitivity and selectivity of the sensing platform, the excellent reproducibility, the stability for continuous assays for over one week and the very good performance in tests using a complex matrix such as commercial milk, convert the proposed Fe_3O_4∩graphite sensor in a very good promise for practical applications in real biological samples.

Acknowledgements

The authors acknowledge partial financial support for this research from Secyt-UNC, UBACyT, ANPCyT (PICT-2015 0077) and CONICET. The authors thank Dr. Silva and Dr. Pereira for assisting with Raman and TEM measurements, respectively.

References

[1] Behrens S., Appel I., Magnetic nanocomposites, *Current. Op. In Biotech.*, **2016**, 39, 89-96.

[2] Lim W. Q., Phua S. Z. F., Xu H. V., Sreejith S., Zhao Y., Recent advances in multifunctional silica-based hybrid nanocarriers

for bioimaging and cancer therapy, *Nanoscale*, **2016**, 8, 12510-12519.

[3] Povolotskaya A. V., Povolotskiy A. V., Manshina A. A., Hybrid nanostructures: synthesis, morphology and functional properties,, *Russian Chemical Reviews*, **2015**, 84, 579-600.

[4] Mallakpoura S., Khadema E., Carbon nanotube–metal oxide nanocomposites: Fabrication, properties and applications, *Chem, Eng. Journal*, **2016**, 302, 344–367.

[5] Pagliaro M., Nedelec J. M., Hybrid materials, *Nanoscale*, **2014**, 6, 6219-6219.

[6] Buehler M. J., Rabu P., Taubert A., Advanced Hybrid Materials: Design and Applications, *Eur. J. Inorg. Chem.*, **2012**, 32, 5092-5093.

[7] Diaz-Diestra D., Thapa B., Beltran-Huarac J., Weiner B. R., Morell G., L-cysteine capped ZnS:Mn quantum dots for room-temperature detection of dopamine with high sensitivity and selectivity, *Biosens Bioelectron*, **2017**, 87, 693–70.

[8] Campbell A. S., Murata H., Carmali S., Matyjaszewski K., Islam M. F., Russell A. J., Polymer-based protein engineering grown ferrocene-containing redox polymers improve current generation in an enzymatic biofuel cell, *Biosens Bioelectron*, **2016**, 85, 446–453.

[9] Tala-Ighil R., Nanomaterials in Solar Cells, Handbook of Nanoelectrochemistry, Springer International Publishing Switzerland, **2015**.

[10] Zheng, X., Wang, Y., Sun, L., TbF_3 nanoparticles as dual-mode contrast agents for ultrahigh field magnetic resonance imaging and X-ray computed tomography, *Nano Res*, **2016**, 9, 1135–1147.

[11] Kang N., Park J.H., Choi J., Jin J., Chun J., Jung I. G., Jeong J., Park J. G., Lee S. M., Kim H. J., Son S. U., Nanoparticulate iron oxide tubes from microporous organic nanotubes as stable anode materials for lithium ion batteries, A*ngew Chem*, **2012**, 51, 6626–6630.

[12] El Ghandoor H., Zidan H. M., Khalil M. M. H., Ismail M. I. M., Synthesis and Some Physical Properties of Magnetite (Fe_3O_4) Nanoparticles, *Int. J. Electrochem. Sci.*, **2012**, 7, 5734 – 5745.

[13] Eshraghi M., Kameli P., Structural and Magnetic Properties of $La_{0.9}Sr_{0.1}MnO_3$ Micro and Nanometer-Sized Manganite Samples, *J. Mater. Sci. Research*, **2014**, 3, 1-7.

[14] Hu X., Wang C., Hydrogen peroxide sensor based on a stainless steel electrode coated with multi-walled carbon nanotubes modified with magnetite nanoparticles, *Microchim. Acta*, **2012**, 179, 329–335.

[15] Chairam S., Sroysee W., Boonchit C., Kaewprom C., Wangnoi T. G. N., Amatatongchai M., Jarujamrus P., Tamaung S., Somsook E., Nonenzymatic Sensor for Hydrogen Peroxide using a Carbon Paste Electrode Modified with a Composite Consisting of Silver Nanoparticles, poly(o-aminobenzoic acid) and Magnetite, *Int. J. Electrochem. Sci.*, **2015**, 10, 4611-4625.

[16] a) Abdalla A. M., Ghosh S., Puri I. K., Decorating carbon nanotubes with co-precipitated magnetite nanocrystals, *Diam Relat Mater,* **2016**, 66, 90–97. b) Thandavan K., Gandhi S., Nesakumar N., Sethuraman S., Rayappan J. B. B., Krishnan U. M., A novel nano-interfaced superoxide biosensor , *Sens. Actuators, B*, **2015**, 215, 166-173.

[17] Osouli-Bostanabada K., Aghajania H., Hosseinzadeb E., Maleki-Ghalehc H., Shakerid M., High Microwave Absorption of Nano-Fe_3O_4 Deposited Electrophoretically on Carbon Fiber, P*rocess. Manuf. Sci.,* **2016**, 31, 1351-1356.

[18] Snovski R., Grinblat J., Margel S., Novel magnetic Fe onion-like fullerene micrometer-sized particles of narrow size distribution, *J. Magn. Magn. Mater.,* **2012**, 324, 90–94.

[19] Zhu S., Guo J., Dong J., Cui Z., Lu T., Zhu C., Zhang D., Ma J., Sonochemical fabrication of Fe_3O_4 nanoparticles on reduced graphene oxide for biosensors, *Ultrason Sonochem*, **2013**, 20, 872-880.

[20] McCreery R. L., Cline K. K., Carbon Electrodes, Chapter 10; Laboratory Techniques in Electroanalytical Chemistry; 2nd Edition, P. T. Kissinger & W. R. Heineman; Marcel Dekker, Inc.; New York, U.S.A., **1996**.

[21] Bracamonte M. V., Melchionna M., Giuliani A., Nasi L., Tavagnacco C., Prato M., Fornasiero P., H_2O_2 sensing enhancement by mutual integration of single walled carbon nanohorns with metal oxide catalysts: The CeO_2 case, *Sens. Actuators B Chem,* **2017**, 239, 923–932.

[22] Holkar C. R., Jadhav A. J., Pinjari D. V., Mahamuni N. M., Pandit A. B., A critical review on textile wastewater treatments: Possible approaches, *J. Environ. Manage.*, **2016**, 182, 351–366.

[23] Zhang L., Chen M., Jiang Y., Chen M., Ding Y., Liu Q., A facile preparation of montmorillonite-supported copper sulfide nanocomposites and their application in the detection of H_2O_2, *Sens. Actuators B Chem*, **2017**, 239, 28–35.

[24] Malinouski M., Zhou , Y. Belousov V. V., Hatfield D. L., Gladyshev V. N., Hydrogen Peroxide Probes Directed to Different Cellular Compartments, *PLoS ONE*, **2011**, 6, 1-10.

[25] a) Sarroca S., Molina-Martínez P., Aresté C., Etzrodt M., García de Frutos P., Gasa R., Antonell A., Molinuevo J. L., Sánchez-Valle R., Saura C. A., Lladó A., Sanfeliu C., Preservation of cell-survival mechanisms by the presenilin-1 K239N mutation may cause its milder clinical phenotype, *Neurobiol. Aging*, **2016**, 46, 169–179. b) Kich D. M., Bitencourt S., Alves C., Silva J., Pinteus S., Pedrosa R., Laufer S., Volken de Souza C. F., Goettert M. I., Neuromodulatory effects of *Calyptranthes grandifolia* extracts against 6-hydroxydopamine-induced neurotoxicity in SH-SY5Y cells, *Biomed Pharmacother*, **2016**, 84, 382–386.

[26] Koppenhöfer D., Kettenbaum F., Susloparova A., Law J. K. Y., Vu X. T., Schwab T., Schäfer K. H., Ingebrandt S., Neurodegeneration through oxidative stress: Monitoring hydrogen peroxide induced apoptosis in primary cells from the subventricular zone of BALB/c mice using field-effect transistors, *Biosens Bioelectron*, **2016**, 67, 490–496.

[27] a) Zhou B., Wang J., Guo Z., Tan H., Zhu X., A simple colorimetric method for determination of hydrogen peroxide in plant tissues, *Plant Growth Reg.*, **2006**, 49, 113-118. b) Gimeno P., Bousquet C., Lassu N., Maggio A., Civade C., Brenier C., Lempereur L., High-performance liquid chromatography method for the determination of hydrogen peroxide present or released in teeth bleaching kits and hair cosmetic product,.*J. Phar. and Biom. Anal.*, **2015**, 107 386–393. c) Magalhães L. M., Lúcio M., Segundo M. A., Reis S., Lima J. L. F. C., Automatic flow injection based methodologies for determination of scavenging capacity against biologically relevant reactive species of oxygen and nitrogen, *Talanta*, **2009**, 78, 1219–1226. d) Fernández-Ramos M. D., Ordóñez Y. F., Capitán-Vallvey L. F., Pérez de Vargas-Sansalvador I. M., Ballesta-Claver J., Optical humidity sensor using methylene blue immobilized on a hydrophilic polymer*, Sens. Actuators B Chem*, **2017**, 241, 528–533.

[28] Yeh M. H., Li Y. S., Chen G. L., Lin L. Y., Li T. J., Chuang H. M., Hsieh C. Y., Lo S. C., Chiang W. H., Ho K. C., Facile Synthesis of Boron-doped Graphene Nanosheets with Hierarchical Microstructure at Atmosphere Pressure for Metal-free Electrochemical Detection of Hydrogen Peroxide, *Electrochim. Acta,* **2015**, 172, 52–60.

[29] Wang N., Zhu L., Wang D., Wang M., Lin Z., Tang H., Fe_3O_4–MWCNT magnetic nanocomposites as efficient peroxidase mimic catalysts in a Fenton-like reaction for water purification without pH limitation*, Ultrason Sonochem*, **2010**, 17, 526–533.

[30] Zhang J., Xia Z., Dai L., Carbon-based electrocatalysts for advanced energy conversion and storage, *Sci. Adv.*, **2015**, 1, e1500564.

[31] Andradea Â. L., Valentec M. A., Ferreira J. M. F., Fabris J. D., Preparation of size-controlled nanoparticles of magnetite*, J. Magn. Magn. Mater.*, **2012**, 324, 1753–1757.

[32] Upadhyaya S., Parekhb K., Pandey B., Influence of crystallite size on the magnetic properties of Fe_3O_4 nanoparticles*, J. Alloy. Comp.*, **2016**, 678, 478–485.

[33] Shebanova O. N., Lazor P., Raman spectroscopic study of magnetite (Fe_2O_4): a new assignment for the vibrational spectrum*, J. Solid. State Chem.*, **2003**, 174, 424-430.

[34] Jorio, A.; Dressehlhaus, M.; Saito, R.; Dresselhaus, G. F. Raman Spectroscopy in Graphene Related Systems; Wiley-VCH: Weinheim, Germany, **2011**.

[35] Chandramohan P., Srinivasan M. P., Velmurugan S., Narasimhan S. V., Cation distribution and particle size effect on Raman spectrum of $CoFe_2O_4$, *J. Solid. State Chem.,* **2011**, 184, 89–96.

[36] Zhao X., Wang W., Zhang Y., Wu S., Li F., Liu J. P., Synthesis and characterization of gadolinium doped cobalt ferrite nanoparticles with enhanced adsorption capability for Congo Red, *Chem. Eng. Journal,* **2014**, 250, 164-174.

[37] Mishra A. K., Ramaprabhu S., Magnetite decorated graphite nanoplatelets as cost effective CO_2 adsorbent, *J. Mater. Chem.*, **2011**, 21, 7467-7471.

[38] Reich S., Thomsen C., Raman spectroscopy of graphite, *Phil. Trans. R. Soc. Lond. A*, **2004**, 362, 2271–2288.

[39] Bracamonte M. V., Lacconi G. I., Urreta S. E., Foa Torres L. E. F., On the Nature of Defects in Liquid-Phase Exfoliated Graphene*, J. Phys. Chem C.*, **2014**, 118, 15455-15459.

[40] Eckmann A., Felten A., Verzhbitskiy I., Davey R., Casiraghi C., Probing the Nature of Defects in Graphene by Raman Spectroscopy, *Nano Lett.*, **2012**, 12, 3925-3930.

[41] Yang J., Xiang H., Shuai L., Gunasekaran S., A sensitive enzymeless hydrogen-peroxide sensor based on epitaxially-grown Fe_3O_4 thin film*, Anal. Chim. Acta*, **2011**, 708, 44-51.

[42] Miao Z., Zhang D., Chen Q., Non-enzymatic Hydrogen Peroxide Sensors Based on Multi-wall Carbon Nanotube/Pt Nanoparticle Nanohybrids, *Materials,* **2014**, 7, 2945-2955.

[43] Dutta A. K., Maji S. K., Srivastava D. N., Mondal A., Biswas P-, Paul P., Adhikary B., Peroxidase-like activity and amperometric sensing of hydrogen peroxide by Fe_2O_3 and Prussian Blue-modified Fe_2O_3 nanoparticles*, J. Mol. Catal. A: Chem*, **2012**, 360, 71-77.

[44] Jaime-González J., Marzario E., Menendez N., Sanchez-Marcos J., Muñoz-Bonilla A., Herrasti P., Comparison of ferrite nanoparticles obtained electrochemically for catalytical reduction of hydrogen peroxide*, J Solid State Electrochem*, **2015**, 1- 8.

[45] Jakubec P., Urbanová V., Marková Z., Zbořil R., Novel Fe@Fe-O@Ag nanocomposite for efficient non-enzymatic sensing of hydrogen peroxide*, Electroch. Acta*, **2015**, *153*, 62-?.

[46] Lin C-Y. Chang C-T., Iron oxide nanorods array in electrochemical detection of H_2O_2 *Sens. Actuat. B*, **2015**, 220, 695-704.